


# Osmotic Delivery and Release of Lipid-Encapsulated Molecules via Sequential Solution Exchange

Sangwoo Shin,<sup>1,\*</sup> Viet Sang Doan,<sup>1</sup> and Jie Feng<sup>2</sup>

<sup>1</sup>*Department of Mechanical Engineering, University of Hawaii at Manoa, Honolulu, Hawaii 96822, USA*

<sup>2</sup>*Department of Mechanical Science and Engineering, University of Illinois at Urbana–Champaign, Urbana, Illinois 61801, USA*

 (Received 21 November 2018; revised manuscript received 22 April 2019; published 8 August 2019)

Passive targeted drug delivery to solid tumors is driven by the permeation of drug carriers through porous vasculature. Due to a dominant transport mechanism for the entry and migration of the drug carriers being diffusion, the passive drug delivery is relatively slow and ineffective in delivering large carriers to the desired location. Here, we propose a method for delivering liposomes into the interstitium at orders of magnitude faster than the diffusion. Using microfluidic model tumor microenvironment, we show that by exchanging the solutes of the interstitial fluid, the liposomes can respond to the change in the chemistry of the surrounding fluid, thereby penetrating deep into the confined pore space at an accelerated transport rate. In addition, by further exchanging the environment with a hypotonic solution, the delivered liposomes can expel their inner content continuously via periodic osmotic bursting, allowing controlled release of encapsulated molecules in hard-to-reach spaces. Our study suggests an active delivery strategy to enhance the permeation of therapeutic molecules into the interstitium.

DOI: [10.1103/PhysRevApplied.12.024014](https://doi.org/10.1103/PhysRevApplied.12.024014)

## I. INTRODUCTION

Current understanding of passive targeted drug delivery relies on the enhanced permeation and retention (EPR) effect, a mechanism by which the drugs can penetrate through the porous vasculature, followed by accumulation within the solid tumors [1,2]. Due to the endothelium of the vasculature around the tumor being more permeable than its normal state [3], the drug carriers are able to migrate spontaneously into the tumor interstitium during their circulation in blood. In addition, the compressed tumor matrix and the abnormal lymphatic vessels hinder the lymphatic drainage [4], thus enabling the retention of the drug carriers [3,5]. While this EPR effect is known to be a direct way of passively delivering drugs into the tumor, the delivery efficacy is reported to be extremely low where only a fraction of the injected drugs actually ends up in the tumor [2,6].

One of the main reasons for such a low efficacy is attributed to the transport mechanism of the drug carriers. A typical interstitial flow speed within a tumor is reported to be  $\mathcal{O}(0.1 \mu\text{m/s})$  [7–9], which is at least an order of magnitude slower than the rate of diffusion across approximately  $100 \mu\text{m}$  for typical nanoparticles and therapeutic molecules in aqueous environments. In this regard, drug

transport is essentially dominated by diffusion in the tumor interstitium.

To exploit diffusion as an effective transport mechanism, drug carriers need to be small since the diffusivity is inversely proportional to their size. Unfortunately, small carriers exhibit relatively short circulation lifetime due to a number of reasons such as renal filtration, fast enzymatic degradation, and accumulation in nontargeted organs and tissues, thus limiting the availability of drug carriers for the delivery [3]. Small carriers also have the risk of diffusing back to the circulation [1,3]. In this regard, relatively large (diameter  $> 100 \text{ nm}$ ) drug carriers are preferred for passive drug delivery [2]. However, large carriers are also ineffective in penetrating into the tumor via passive diffusion due to their small diffusivity. The physical confinement of the interstitial matrix further reduces the effective diffusivity of large carriers [10]. Moreover, diffusion is spatially monotonic such that the number of carriers will gradually decrease as they penetrate into the tumor. Thus it is unfeasible to accumulate a large number of drug carriers in the tumor matrix by diffusion, particularly if the carriers are dilute, which occurs over time during circulation. In consequence, less than 1% of the injected drugs are known to accumulate successfully in the tumor while the rest ending up elsewhere in the body [6].

In this regard, the goal of this paper is to demonstrate a potential strategy for enhancing the migration of large drug carriers in terms of transport rate and number density by

\*sangwoos@hawaii.edu

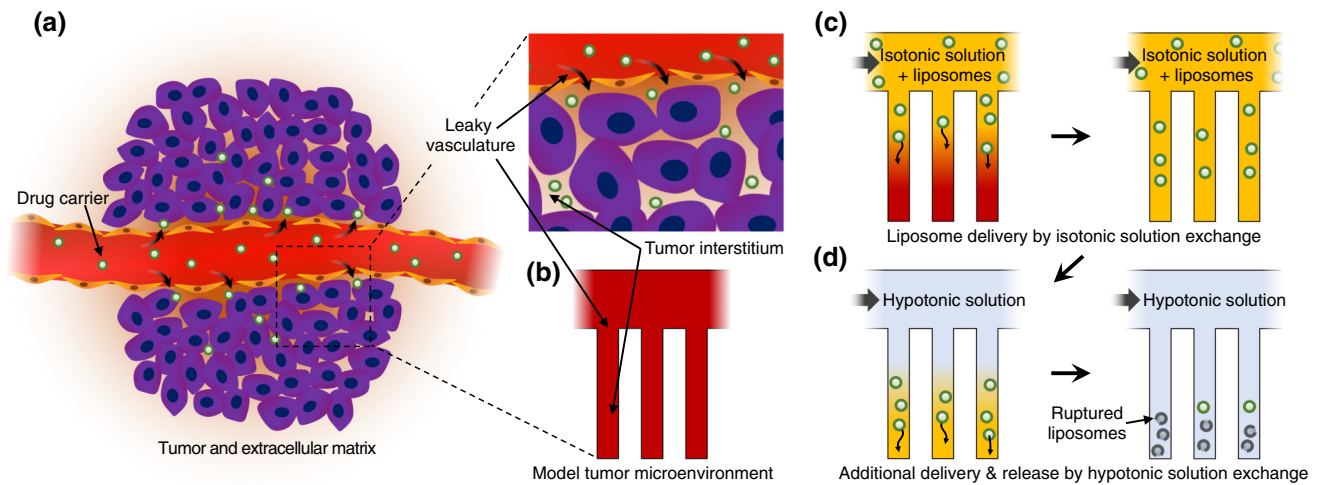


FIG. 1. Fast delivery and triggered release of drug carriers in tumor interstitium by sequential solution exchange. (a) Passive drug delivery in solid tumors by EPR effect. (b) The porous vasculature and the confined tumor interstitium is modeled as a series of dead-end pores connected to a large flow channel. (c) In this setup, liposomes can be delivered into the dead-end pores at an accelerated rate by flowing an isotonic solution through the main channel so that the liposomes remain intact while migrating into the pores by diffusiophoresis. (d) Subsequently a hypotonic solution is flowed through the flow channel. The osmotic imbalance between the inner content of the liposomes and the solution triggers a release of the inner content of the liposomes by osmotic bursting. Simultaneously, the liposomes further migrate into the pores by diffusiophoresis due to another solute gradient established by the diffusion of the hypotonic solution.

sequentially exchanging the solutes in the interstitium. By injecting a suspension of drug carriers containing different solutes than the interstitial fluid to the nearby host vessels, solute gradients can be established within the tumor interstitium. This may allow the carriers to respond to the gradients and thereby migrate at an accelerated rate via nonequilibrium transport mechanisms such as *diffusiophoresis*. This process allows migration of large colloids at orders of magnitude faster than diffusion [11,12], making it a promising mechanism for the enhanced delivery of large drug carriers. We employ microfluidic devices and liposomes for simulating the delivery of drug carriers into the tumor matrix via the proposed strategy. Furthermore, a subsequent injection of hypotonic solution triggers the release of the inner content of the liposomes by osmotic bursting. Our results suggest a noninvasive method for delivering and releasing encapsulated molecules in hard-to-reach spaces in a controlled manner.

## II. MATERIALS AND METHODS

1,2-dioleoyl-*sn*-glycero-3-phosphocholine (DOPC) and 1,2-dipalmitoyl-*sn*-glycero-3-phosphoethanolamine-*N*-(lisamine rhodamine B sulfonyl) (ammonium salt) (Rh-DPPE) are purchased from Avanti Polar Lipids. Sucrose, NaCl, phosphate-buffered saline (PBS) are purchased from Sigma-Aldrich. The microfluidic devices are made with polydimethylsiloxane (PDMS; Sylgard 184, Dow Corning) via a standard soft lithography [13]. DOPC liposomes labeled with Rh-DPPE are synthesized using the

electroformation method [14,15]. In brief, 10  $\mu\text{g}$  of a mixture of DOPC and Rh-DPPE (99.5/0.5 mol% in chloroform) is dried on the surfaces of two ITO-coated slide glasses (Delta Technologies) overnight in a vacuum chamber. The dried lipids are rehydrated with 0.3M sucrose solution in a chamber made out of the ITO glass slides separated by a PDMS gasket (thickness = 5 mm). An ac electrical field (1.75 V<sub>pp</sub>, 10 Hz) is applied to the ITO glass slides for 12 h to form the liposomes. The size and the zeta potential of the liposomes is measured using an electrophoretic light-scattering technique (Zetasizer Nano ZS, Malvern).

Experiments for visualizing swell-burst events of liposomes (Figs. 2 and 3) are performed in a chamber made by puncturing a hole (diameter = 6 mm) in a slab of PDMS and placing it on a clean slide glass. A small volume of

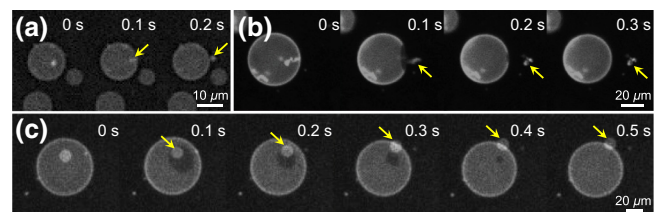


FIG. 2. Releasing the inner content of liposomes by osmotic bursting. The DOPC liposomes expel their inner content (0.3M sucrose) upon exposure to hypotonic solution (deionized water). (a)–(c) Image sequence of the osmotic bursting in liposomes with different sizes. Sudden ejections of the inner content are observed, which are marked with yellow arrows.

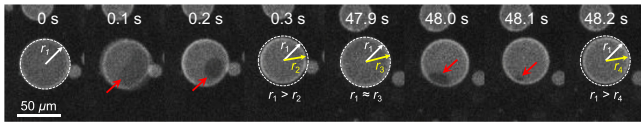


FIG. 3. Periodic osmotic swell-burst cycle. Upon exposure to isotonic solution (deionized water), a liposome with initial radius of  $r_1$  partially ruptures (marked with red arrows) and expels its inner content ( $0.3M$  sucrose), resulting in a decrease in the radius of the liposome ( $r_1 > r_2$ ). After the ruptured membrane is resealed, the liposome continues to grow, to a size similar to the initial radius ( $r_1 \approx r_3$ ), until the internal pressure reaches the membrane lysis tension. Subsequently, the liposome shrinks again ( $r_1 > r_4$ ) due to another burst process.

liposome suspension is first loaded in the chamber, followed by a gentle injection of hypotonic solution (deionized water) with a volume ten times larger than that of the liposome solution using a micropipette.

Liposome-delivery experiments (Figs. 4 and 5) are performed in a microfluidic device that consists of a straight main channel with height  $\times$  width =  $100 \times 200 \mu\text{m}^2$  and multiple dead-end pores with height  $\times$  width  $\times$  length =  $40 \times 48 \times 800 \mu\text{m}^3$  that are placed normal to the main channel [12,15]. Initially, the channels are filled with a saline solution ( $0.16M$  NaCl or PBS). Subsequently, the liposome suspension is fed through the main channel with a syringe pump (Pump 11 Pico Plus Elite, Harvard Apparatus), creating a transient solute gradient across the dead-end pores. After the solutes are equilibrated so that the liposomes do not show any directed motion, a hypotonic solution (deionized water) is injected through another inlet of the main flow channel using another syringe pump in order to trigger swell bursting inside the pores. The liposomes are visualized with an inverted fluorescence microscope (DMi8, Leica) and analyzed with ImageJ and Matlab.

### III. RESULTS AND DISCUSSION

A typical scenario illustrating the delivery of drug carriers into the tumor via the EPR effect is presented in Fig. 1(a). Increased permeability of the endothelium of the vasculature allows the drug carriers to enter the tumor interstitium. Due to the lack of fluid flow in the tumor matrix, the permeable vasculature and the interstitium can be effectively considered as deep dead-end pore spaces connected to a larger flow channel as shown in Fig. 1(b). While the actual width of the pores in the endothelium is reported to be less than a micron [16,17], we use an upscaled microfluidic setup that mimics the geometry of a tumor microenvironment for testing and visualizing the delivery and release of lipid-encapsulated molecules using a conventional optical microscope.

Our strategy for overcoming the slow diffusion of drug carriers is to exploit the fast diffusion of molecular solutes.

When a large colloidal particle is exposed to a local solute gradient, it can experience an accelerated migration along the solute gradient by *diffusiophoresis* [18,19], which has gained a renewed interest in the recent years [20,21]. Although the majority of the literature on diffusiophoresis is focused on the motion of solid particles, it is also well known that soft colloids such as liposomes and immiscible drops can undergo diffusiophoresis [22,23].

While diffusiophoresis occurs in both electrolyte and nonelectrolyte solutions, electrolytes with large diffusivity contrast among the solute species can induce a strong *electrolytic diffusiophoresis* for charged colloids [18]. The electrolytic diffusiophoresis velocity is given as  $\mathbf{u}_p = \Gamma_p \nabla \ln c$  where  $\Gamma_p$  is the diffusiophoretic mobility and  $c$  is the solute concentration. For an infinitesimally thin Debye layer, which is a valid approximation for relatively concentrated solutions (e.g., physiological fluids), the diffusiophoretic mobility  $\Gamma_p$  is independent of the particle size and shape [18,19]. For 1:1 electrolyte, the diffusiophoretic mobility is given as  $\Gamma_p = (\epsilon V_T^2 / \eta) [(\beta \zeta / V_T) + 4 \ln \cosh(\zeta / 4V_T)]$ , where  $\epsilon$  is the solution permittivity,  $\eta$  is the solution viscosity,  $\zeta$  is the colloid zeta potential,  $V_T = kT/e$  is the thermal voltage,  $k$  is the Boltzmann constant,  $T$  is the temperature, and  $e$  is the electron charge.  $\beta = (D_+ - D_-) / (D_+ + D_-)$  is the dimensionless diffusivity contrast between the cation ( $D_+$ ) and the anion ( $D_-$ ).

By creating solute gradients within the interstitium, the liposomes in the blood vessel can migrate into the tumor via diffusiophoresis [Fig. 1(c)]. While electrolytic solutes are naturally present in the interstitial fluid that may enable electrolytic diffusiophoresis [24], liposomes are semipermeable such that they experience osmosis when exposed to a solute gradient, which could result in the damage of the liposomes even before entering the dead-end pores. In this regard, by injecting a nonelectrolyte solution having an identical osmolarity as the interstitial fluid, electrolytic diffusiophoresis can still occur without the risk of experiencing osmotic shock, thereby allowing the liposomes to safely migrate into the deep pores.

Once the liposomes have migrated into the pores, a further exchange of solutes with a hypotonic solution can be made in order to release the inner content of the liposomes by osmotic bursting [Fig. 1(d)]. This process not only forces the liposomes to expel out their inner content, but also allows the liposomes to further migrate into the pore via *nonelectrolytic diffusiophoresis*. We use this sequential exchange strategy to enhance the delivery and release of the lipid-encapsulated molecules.

To first test the feasibility of utilizing osmosis for releasing the inner content of liposomes, we observe the rupture dynamics of liposomes under hypotonic condition in an enclosed fluid chamber. We use DOPC liposomes labeled with Rh-DPPE, which makes the liposomes negatively charged (zeta potential approximately equal to  $-89$  mV

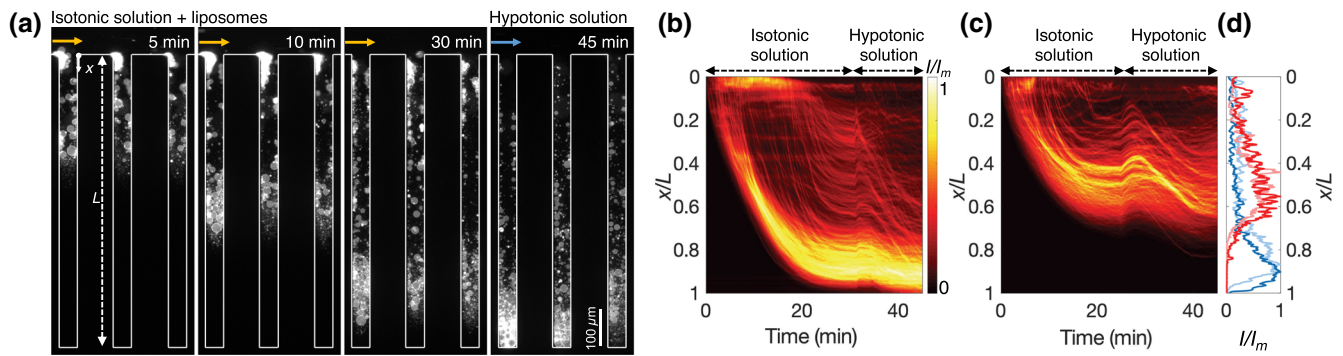


FIG. 4. Liposome delivery in dead-end pores by sequential exchange of solutions. (a) Image sequence of DOPC liposomes migrating into the microscale dead-end pores upon exposure to an isotonic solution followed by a hypotonic solution. A suspension of liposomes in  $0.3M$  sucrose solution is flowed over an array of dead-end pores (length,  $L = 800 \mu\text{m}$ ) containing  $0.16M$  NaCl. Subsequently, the flow channel is flushed with a hypotonic solution (deionized water) to induce osmotic bursting and additional migration of liposomes into the pores. (b),(c) Spatiotemporal diagrams of fluorescence intensity averaged over five pores normalized by the maximum intensity,  $I/I_m$ . The dead-end pores are initially filled with (b)  $0.16M$  NaCl or (c) PBS solution. Color represents fluorescence intensity, which effectively represents a number density of liposomes. (d)  $I/I_m$  from (b) (blue) and (c) (red) at 25 min (faint-colored curves) and 45 min (bright-colored curves).

in  $10 \text{ mM}$  NaCl). The liposomes are formed via electroformation in  $0.3M$  sucrose solution [14]. The size of the liposomes is observed to be highly dispersed, ranging from  $0.1$  to  $50 \mu\text{m}$  in diameter. Upon exposure to hypotonic solution, water permeates into the liposomes by osmosis, causing them to swell and then rupture once the membrane tension exceeds the critical lysis tension.

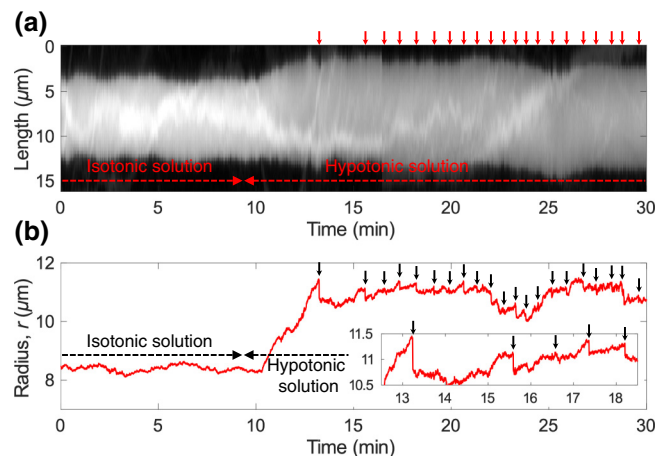


FIG. 5. Periodic swell bursting of a liposome containing  $0.3M$  sucrose solution in a dead-end pore upon exposure to hypotonic solution (deionized water). (a) Spatiotemporal diagram of averaged images of a single liposome in a dead-end pore. The image is reproduced using Matlab such that the liposome is located in the center of the image throughout for better comparison of its size over time. (b) Radius of the liposome shown in (a) over time. Inset shows a closer view of the radius after the initial burst. The liposome radius is analyzed by tracking the liposome using the Mosaic plugin in ImageJ [40]. The arrows in (a),(b) represent individual burst events.

It is well known that the liposomes synthesized by electroformation often result in multilamellar liposomes, containing smaller liposomes inside of them [25]. This feature allows us to visualize the ejection process where the smaller liposomes effectively serve as passive tracers as shown in Fig. 2 (see also Movie S1 within the Supplemental Material [26]). Due to the osmotic pressure, the liposome ruptures for a short period of time during which the inner content (yellow arrows in Fig. 2) expels out at the maximum speed of approximately  $200 \mu\text{m/s}$  until the ruptured membrane is resealed. Although the duration time for the forced ejection occurs on the order of  $0.1 \text{ s}$ , this time scale is observed to be size dependent in which the larger liposomes tend to experience longer time to reseat the ruptured membrane, agreeing with previous reports [27–29].

This burst release mechanism is not only rapid, but is also continuous in the sense that the swell-burst event occurs periodically over time. Since the inner content does not completely expel out during a single burst event, the osmotic pressure of the inner fluid still remains higher than the outer fluid. This allows another cycle of swell-burst dynamics immediately after the ruptured membrane is resealed, as shown in Fig. 3 (see also Movie S2 within the Supplemental Material [26]). Subsequently, the liposomes experience these dynamics multiple times until the system has reached equilibrium [27,29].

As we confirm the possibility of utilizing osmosis for releasing the inner content of liposomes on demand, we now test the delivery and release of liposomes in a dead-end microfluidic device that mimics the tumor microenvironment. As illustrated in Fig. 1(b), the dead-end pores mimicking the interstitial space are connected to a larger flow channel that represents the permeable mother vessel.

The actual geometry of the device is shown in Fig. 4(a). Along the main flow channel (height  $\times$  width =  $100 \times 200 \mu\text{m}^2$ ), a series of dead-end pores (height  $\times$  width  $\times$  length =  $40 \times 48 \times 800 \mu\text{m}^3$ ) are connected perpendicular to the flow direction. Initially, the channel is completely filled with saline solution ( $0.16M$  NaCl). Then, the channel is flushed with an isotonic, nonelectrolyte solution ( $0.3M$  sucrose) containing liposomes. The detailed experimental procedure can be found in Sec. II.

It should be noted that while the actual tumor interstitium is a complex fluid, which is mainly a hydrogel [30], we model the interstitium as a pure Newtonian fluid. This is justified by the fact that the diffusivity of molecular solutes in hydrogels is similar to that in a free aqueous environment [10,31]. Since diffusiophoresis is a nonequilibrium microscopic process that relies on the diffusion of solutes, the diffusiophoresis velocity is expected to be of the same order of magnitude in both settings. Furthermore, owing to the nature of phoretic swimming, the hydrodynamic retardation due to the confinement of the pore wall is insignificant [19,32]. Such unique characteristics of diffusiophoresis allow us to model the interstitium as an unbounded aqueous environment.

As the liposome suspension flows over the dead-end pores, the contrast in the solutes between the pores and the main channel results in the interdiffusion of multiple solutes. Assuming semi-infinite diffusion at infinite dilution, the osmolarity inside the pores can be approximated as  $n \approx n_0 [\text{erfc}(x/\sqrt{4D_N t}) + \text{erf}(x/\sqrt{4D_S t})]$ , where  $x$  is the porewise direction,  $n_0$  is the initial osmolarity of the solutions ( $0.3 \text{ Osm/L}$ ), and  $D_N$  and  $D_S$  are the diffusivities of NaCl and sucrose, respectively. Due to the difference in their diffusivities ( $D_N = 1.6 \times 10^{-9} \text{ m}^2/\text{s}$ ,  $D_S = 0.5 \times 10^{-9} \text{ m}^2/\text{s}$  [33,34]), a local fluctuation in the osmolarity arises where the solution can be slightly hypertonic (approximately  $0.38 \text{ Osm/L}$ ) near the sucrose diffusion front. This may lead to a temporal loss of the inner fluid to some extent, but should not influence the diffusiophoretic motion of the liposomes significantly due to the size- and shape-independent characteristics of diffusiophoresis [18,19]. It is also shown in Fig. 4(a) that the liposomes migrate at a similar rate regardless of their size (see also Movie S3 within the Supplemental Material [26]). Eventually, the liposomes swell back to their original shape as the solute reaches equilibrium at  $0.3 \text{ Osm/L}$ . Therefore, the liposomes remain intact during their migration into the pores as shown in Fig. 4(a).

The transient migration of liposomes is also presented in Fig. 4(b) by plotting the distribution of the width-averaged fluorescence intensity normalized by the maximum intensity ( $I/I_m$ ) over time. Here, the slope of the liposome trajectories represents the velocity of the liposomes where they initially migrate at approximately  $20 \mu\text{m/s}$ , which is 2 orders of magnitude faster than the average interstitial flow velocity [7,8].

Furthermore, due to the logarithmic characteristics of diffusiophoresis [35,36], i.e.,  $\mathbf{u}_p \sim \nabla \ln c$ , the trailing liposomes catch up the leading ones as they travel into the pores, resulting in an accumulation of liposomes near the solute diffusion front [Fig. 4(a)]. This feature makes the diffusiophoresis more desirable for targeted delivery since the liposomes can be spontaneously preconcentrated during the delivery process. The strong accumulated front is also observed in Figs. 4(b) and 4(d) where Fig. 4(d) shows  $I/I_m$  at 25 min (faint blue curve).

It should be noted that in the presence of NaCl-sucrose gradients, there are multiple possible migration mechanisms that may contribute to the directed liposome motion such as electrolytic diffusiophoresis, nonelectrolytic diffusiophoresis, and osmophoresis [19,37]. For semipermeable, charged liposomes under NaCl-sucrose gradients at constant osmolarity, both the electrolytic and nonelectrolytic diffusiophoresis may arise whereas osmophoresis can be neglected due to the absence of osmolarity gradient. The migration direction for a negatively charged liposome in the current system is opposite for the electrolytic and nonelectrolytic diffusiophoresis. However, as mentioned earlier, electrolytic diffusiophoresis tends to be more significant than the nonelectrolytic diffusiophoresis, particularly when the electrolytes have a large diffusivity contrast  $\beta$  such as NaCl, LiCl, and  $\text{H}_2\text{CO}_3$  [11,12,38]. For example, the nonelectrolytic diffusiophoresis velocity due to the sucrose gradient is  $u \approx (kT\lambda_S^2\Delta c/\eta\lambda_G) \sim \mathcal{O}(1 \mu\text{m/s})$ , where  $\lambda_G$  is the length scale of the gradient and  $\lambda_S$  is the solute-colloid interaction length, which we assume  $1 \text{ nm}$  [39]. In contrast, the electrolytic diffusiophoresis velocity of the liposome due to the NaCl gradient is  $u \approx (\Gamma_p/\lambda_G) \sim \mathcal{O}(10 \mu\text{m/s})$ , which is an order of magnitude faster than the nonelectrolytic diffusiophoresis. In consequence, the liposomes migrate *into* the deep pores.

Once the gradient has ceased out, a hypotonic solution is subsequently injected through the main flow channel to induce osmotic bursting. The introduction of deionized water creates sucrose gradient within the pores, enabling further migration of liposomes via nonelectrolytic diffusiophoresis. Although this migration mechanism is typically weaker than the electrolytic diffusiophoresis experienced by NaCl gradient as mentioned, it can still contribute to the additional migration of liposomes further *into* the pores. We note that the sudden reversal of the motion of the liposomes at the time of solution exchange [approximately 30 min in Fig. 4(b)] is due to the small amount of initial saline solution remaining in the upstream of the flow channel while switching the solutions, due to the geometry of the microfluidic setup having two separate inlets. This however lasts only for a few minutes before the hypotonic solution is completely spread out in the flow channel.

As the sucrose molecules diffuse out from the pores, the liposomes start to migrate again into the pores via nonelectrolytic diffusiophoresis. Simultaneously, the liposomes

begin to expel inner fluid by periodic bursting. While this burst event cannot be visualized for submicron liposomes via optical microscopy, the large liposomes ( $>10 \mu\text{m}$ ) present in the solution allow for the detailed visualization and quantification of the rupture events. Periodic swell-burst events for a liposome upon exposure to a hypotonic solution inside a dead-end pore is shown in Fig. 5 where the time-lapse morphology of a single liposome [Fig. 5(a)] and its radius [Fig. 5(b)] are presented. We explain below the mechanism of osmotic outburst in this context. Once the solutes start to diffuse out of the pore (after hypotonic flushing), the internal pressure builds up due to the water influx, resulting in an increase of the liposome size (starting at around 10 min). This continues until the membrane tension reaches the critical lysis tension at which the liposome ruptures and expels out some portion of the inner fluid (approximately 5% of initial volume [27]). After the first cycle, the subsequent swell-burst cycles continue periodically for more than 10 min, as indicated by the arrows in Figs. 5(a) and 5(b). Subsequently, the cycle gradually slows down as the concentration of the inner solution becomes identical to that of the outer solution. The event lasts for over 20 min, making it desirable for controlled, programmable release.

We now address the practical implementation of the proposed strategy for drug delivery. The large osmotic pressure difference imposed during osmotic bursting is not of great concern, since mammalian cells can withstand higher osmotic pressure differences than the synthetic liposomes to a certain extent due to their ability to actively regulate the osmotic pressure via channel proteins and exocytosis [41,42]. However, the use of deionized water for the hypotonic solution may not be practical as it may cause a number of side effects to the patients such as hypovolemia, hypotension, and increased intracranial pressure [43,44]. We show below that the hypotonic solution may contain enough solutes to reduce the risk of side effects from change of the local osmolarity while still triggering osmotic bursting. Based on the theoretical work of Koslov and Markin [27], the critical osmotic pressure difference required to initiate pore nucleation in a semipermeable liposomes with radius  $r$  is given as  $\Delta P_c = 3\kappa^{1/3}\gamma^{2/3}r^{-5/3}$ , where  $\kappa$  is the area extension modulus and  $\gamma$  is the membrane line tension. Assuming  $\kappa = 0.25 \text{ N/m}$  [45] and  $\gamma = 10^{-11} \text{ N}$  [46],  $\Delta P_c$  is estimated to be approximately 40 kPa for a phospholipid liposome with a radius of 100 nm. This pressure difference is equivalent to the osmolarity difference of  $\Delta n \approx 0.016 \text{ Osm/L}$ , which translates to  $\Delta c \approx 8.6 \text{ mM}$  for NaCl or approximately 16 mM for sucrose. These values are an order of magnitude lower than the concentration difference imposed in the current study, and they are also smaller than the concentration difference experienced by lactated Ringer's solution, a widely used hypotonic intravenous fluid [47]. Therefore, in light of practical implementation of the proposed strategy for

drug delivery, the hypotonic solution may contain enough solutes to reduce the risk of side effects from change of the local osmolarity.

To address the feasibility of the proposed method in a realistic environment, we test the proposed strategy with PBS solution, which has a similar osmolarity to 0.16M NaCl solution (approximately 0.3 Osm/L), but contains different solutes that are close to the actual interstitial fluid; the results are shown in Fig. 4(c). Since the PBS solution mainly consists of NaCl, we still observe a substantial migration of liposomes into the pores by electrolytic diffusiophoresis including the accumulated front [also shown as red curves in Fig. 4(d)], although not as strong as compared to the case having NaCl only [Fig. 4(b)]. This is due to the presence of other components in the PBS solution such as  $\text{Na}_2\text{HPO}_4$  and KCl, both of which are irrelevant to the migration into the pores. While KCl is known to experience negligible electrolytic diffusiophoresis compared to NaCl due to the small diffusivity contrast  $\beta$  [33],  $\text{Na}_2\text{HPO}_4$  induces diffusiophoresis of negatively charged liposomes in the opposite direction (toward the pore entrance) due to the diffusivity of  $\text{H}_2\text{PO}_4^-$  being smaller than that of  $\text{Na}^+$  [48]. We also note that the slight acidic environment in actual interstitial fluid within the tumor matrix (pH  $\sim 6.5$  [49]) is unlikely to contribute to the directed motion due to the majority of the solutes being NaCl such that  $(\nabla c + \nabla c_H)/(c + c_H) \approx \nabla \ln c$ , where  $c_H$  is the proton concentration [50]. Therefore, the proposed method has the potential to serve as an effective strategy for delivering large drug carriers to solid tumors.

#### IV. CONCLUSION

We demonstrate a method for delivering liposomes into deep pores that mimic the tumor interstitium, and subsequently releasing the inner content on demand by sequentially exchanging the solutes within the pore space. Using a microfluidic device to model the tumor microenvironment, we observe the transient dynamics of liposome delivery and release upon exposure to different solutions. Introduction of an isotonic solution enables the liposomes to safely migrate deep into the pores via electrolytic diffusiophoresis without experiencing any osmotic shock, whereas subsequent flushing of hypotonic solution allows the liposomes to rapidly release their inner content while migrating further into the pores via nonelectrolytic diffusiophoresis. The release dynamics is shown to be periodic such that the liposomes expel the inner fluid over a long period of time. While the conventional targeted delivery relies on passive diffusion of drug carriers to bring them close to the target location in order to trigger the ligand-receptor interactions [2], the proposed strategy opens a new opportunity to *actively* deliver the drug carriers toward the targets by harnessing the local chemistry of the surroundings.

## ACKNOWLEDGMENTS

This material is based upon work partially supported by the National Science Foundation under Grant No. CBET-1930691, and by the Materials Science Consortium for Research and Education (MSCoRE) at the University of Hawaii, a campus-wide initiative sponsored by the Office of the Vice Chancellor for Research and the Office of the Vice Chancellor for Academic Affairs. S.S. acknowledges Bongseop Kwak and Ting Zhu for helpful discussions.

- 
- [1] H. Maeda, J. Wu, T. Sawa, Y. Matsumura, and K. Hori, Tumor vascular permeability and the EPR effect in macromolecular therapeutics: A review, *J. Control. Release* **65**, 271 (2000).
- [2] Y. H. Bae and K. Park, Targeted drug delivery to tumors: Myths, reality and possibility, *J. Control. Release* **153**, 198 (2011).
- [3] V. Torchilin, Tumor delivery of macromolecular drugs based on the EPR effect, *Adv. Drug Deliv. Rev.* **63**, 131 (2011).
- [4] C.-H. Heldin, K. Rubin, K. Pietras, and A. Östman, High interstitial fluid pressure—an obstacle in cancer therapy, *Nat. Rev. Cancer* **4**, 806 (2004).
- [5] A. Ozcelikkale, H. Moon, M. Linnes, and B. Han, In vitro microfluidic models of tumor microenvironment to screen transport of drugs and nanoparticles, *WIREs Nanomed. Nanobiotechnol.* **9**, e1460 (2017).
- [6] S. Wilhelm, A. J. Tavares, Q. Dai, S. Ohta, J. Audet, H. F. Dvorak, and W. C. W. Chan, Analysis of nanoparticle delivery to tumours, *Nat. Rev. Mater.* **1**, 16014 (2016).
- [7] S. R. Chary and R. K. Jain, Direct measurement of interstitial convection and diffusion of albumin in normal and neoplastic tissues by fluorescence photobleaching, *Proc. Natl. Acad. Sci. U.S.A.* **86**, 5385 (1989).
- [8] H. Dafni, T. Israely, Z. M. Bhujwalla, L. E. Benjamin, and M. Neeman, Overexpression of vascular endothelial growth factor 165 drives peritumor interstitial convection and induces lymphatic drain: Magnetic resonance imaging, confocal microscopy, and histological tracking of triple-labeled albumin, *Cancer Res.* **62**, 6731 (2002).
- [9] W. J. Polacheck, J. L. Charest, and R. D. Kamm, Interstitial flow influences direction of tumor cell migration through competing mechanisms, *Proc. Natl. Acad. Sci. U.S.A.* **108**, 11115 (2011).
- [10] S. Ramanujan, A. Pluen, T. D. McKee, E. B. Brown, Y. Boucher, and R. K. Jain, Diffusion and convection in collagen gels: Implications for transport in the tumor interstitium, *Biophys. J.* **83**, 1650 (2002).
- [11] B. Abécassis, C. Cottin-Bizonne, C. Ybert, A. Ajdari, and L. Bocquet, Boosting migration of large particles by solute contrasts, *Nat. Mater.* **7**, 785 (2008).
- [12] S. Shin, E. Um, B. Sabass, J. T. Ault, M. Rahimi, P. B. Warren, and H. A. Stone, Size-dependent control of colloid transport via solute gradients in dead-end channels, *Proc. Natl. Acad. Sci. U.S.A.* **113**, 257 (2016).
- [13] Y. Xia and G. M. Whitesides, Soft lithography, *Angew. Chem.* **37**, 550 (1998).
- [14] M. I. Angelova and D. S. Dimitrov, Liposome electroformation, *Faraday Discuss.* **81**, 303 (1986).
- [15] S. Shin, J. T. Ault, J. Feng, P. B. Warren, and H. A. Stone, Low-cost zeta potentiometry using solute gradients, *Adv. Mater.* **29**, 1701516 (2017).
- [16] S. K. Hobbs, W. L. Monsky, F. Yuan, W. G. Roberts, L. Griffith, V. P. Torchilin, and R. K. Jain, Regulation of transport pathways in tumor vessels: Role of tumor type and microenvironment, *Proc. Natl. Acad. Sci. U.S.A.* **95**, 4607 (1998).
- [17] B. Kwak, A. Ozcelikkale, C. S. Shin, K. Park, and B. Han, Simulation of complex transport of nanoparticles around a tumor using tumor-microenvironment-on-chip, *J. Control. Release* **194**, 157 (2014).
- [18] D. C. Prieve, J. L. Anderson, J. P. Ebel, and M. E. Lowell, Motion of a particle generated by chemical gradients. Part 2. Electrolytes, *J. Fluid Mech.* **148**, 247 (1984).
- [19] J. L. Anderson, Colloid transport by interfacial forces, *Ann. Rev. Fluid Mech.* **21**, 61 (1989).
- [20] D. Velegol, A. Garg, R. Guha, A. Kar, and M. Kumar, Origins of concentration gradients for diffusiophoresis, *Soft Matter* **12**, 4686 (2016).
- [21] H. J. Keh, Diffusiophoresis of charged particles and diffusioosmosis of electrolyte solutions, *Curr. Opin. Colloid Interface Sci.* **24**, 13 (2016).
- [22] A. Kodama, Y. Sakuma, M. Imai, T. Kawakatsu, N. Puff, and M. I. Angelova, Migration of phospholipid vesicles can be selectively driven by concentration gradients of metal chloride solutions, *Langmuir* **33**, 10698 (2017).
- [23] F. Yang, S. Shin, and H. A. Stone, Diffusiophoresis of a charged drop, *J. Fluid Mech.* **852**, 37 (2018).
- [24] N. Fogh-Andersen, B. M. Altura, B. T. Altura, and O. Siggaard-Andersen, Composition of interstitial fluid, *Clin. Chem.* **41**, 1522 (1995).
- [25] J. R. Howse, R. A. L. Jones, G. Battaglia, R. E. Ducker, G. J. Leggett, and A. J. Ryan, Templated formation of giant polymer vesicles with controlled size distributions, *Nat. Mater.* **8**, 507 (2009).
- [26] See Supplemental Material at <http://link.aps.org/supplemental/10.1103/PhysRevApplied.12.024014> for Movies S1, S2, and S3.
- [27] M. M. Koslov and V. S. Markin, A theory of osmotic lysis of lipid vesicles, *J. Theor. Biol.* **109**, 17 (1984).
- [28] O. Sandre, L. Moreaux, and F. Brochard-Wyart, Dynamics of transient pores in stretched vesicles, *Proc. Natl. Acad. Sci. U.S.A.* **96**, 10591 (1999).
- [29] M. Chabanon, J. C. S. Ho, B. Liedberg, A. N. Parikh, and P. Rangamani, Pulsatile lipid vesicles under osmotic stress, *Biophys. J.* **112**, 1682 (2017).
- [30] B. Alberts, A. Johnson, J. Lewis, M. Raff, K. Roberts, and P. Walter, *Molecular Biology of the Cell* (Garland Science, New York, 2007), 5th ed.
- [31] R. K. Jain, Transport of molecules in the tumor interstitium: A review, *Cancer Res.* **47**, 3039 (1987).
- [32] H. J. Keh and J. L. Anderson, Boundary effects on electrophoretic motion of colloidal spheres, *J. Fluid Mech.* **153**, 417 (1985).

- [33] E. L. Cussler, *Diffusion: Mass Transfer in Fluid Systems* (Cambridge University Press, Cambridge, 2009), 3rd ed.
- [34] H. C. Price, J. Mattsson, and B. J. Murray, Sucrose diffusion in aqueous solution, *Phys. Chem. Chem. Phys.* **18**, 19207 (2016).
- [35] J. Palacci, C. Cottin-Bizonne, C. Ybert, and L. Bocquet, Osmotic traps for colloids and macromolecules based on logarithmic sensing in salt taxis, *Soft Matter* **8**, 980 (2012).
- [36] S. Shin, P. B. Warren, and H. A. Stone, Cleaning by Surfactant Gradients: Particulate Removal from Porous Materials and the Significance of Rinsing in Laundry Detergency, *Phys. Rev. Appl.* **9**, 034012 (2018).
- [37] J. L. Anderson, Transport mechanisms of biological colloids, *Ann. N. Y. Acad. Sci.* **469**, 166 (1986).
- [38] S. Shin, O. Shardt, P. B. Warren, and H. A. Stone, Membraneless water filtration using CO<sub>2</sub>, *Nat. Commun.* **8**, 15181 (2017).
- [39] R. P. Sear, Diffusiophoresis in Cells: A General Nonequilibrium, Nonmotor Mechanism for the Metabolism-dependent Transport of Particles in Cells, *Phys. Rev. Lett.* **12**, 128101 (2019).
- [40] MosaicSuite for ImageJ and Fiji. <http://mosaic.mpi-cbg.de/?q=downloads/imageJ>.
- [41] S. N. Ho, Intracellular water homeostasis and the mammalian cellular osmotic stress response, *J. Cell. Physiol.* **206**, 9 (2006).
- [42] M. Sheetz and H. Yu, *The Cell as a Machine* (Cambridge University Press, Cambridge, 2018).
- [43] M. Alexander, A. Corrigan, L. Gorski, J. Hankins, and R. Perucca, *Infusion Nursing: An Evidence-Based Approach* (Saunders, St. Louis, 2010), 3rd ed.
- [44] A. Crawford and H. Harris, I.V. fluids what nurses need to know, *Nursing* **41**, 30 (2011).
- [45] D. Marsh, Elastic curvature constants of lipid monolayers and bilayers, *Chem. Phys. Lipids* **144**, 146 (2006).
- [46] E. Karatekin, O. Sandre, H. Guitouni, N. Borghi, P.-H. Puech, and F. Brochard-Wyart, Cascades of transient pores in giant vesicles: Line tension and transport, *Biophys. J.* **84**, 1734 (2003).
- [47] E. L. Williams, K. L. Hildebrand, S. A. McCormick, and M. J. Bedel, The effect of intravenous lactated Ringer's solution versus 0.9% sodium chloride solution on serum osmolality in human volunteers, *Anesth. Analg.* **88**, 999 (1999).
- [48] J. E. Burkell and J. W. T. Spinks, Measurements of self-diffusion in aqueous solutions of sodium dihydrogen phosphate, *Can. J. Chem.* **30**, 311 (1952).
- [49] L. Feng, Z. Dong, D. Tao, Y. Zhang, and Z. Liu, The acidic tumor microenvironment: A target for smart cancer nanotheranostics, *Natl. Sci. Rev.* **5**, 269 (2017).
- [50] T.-Y. Chiang and D. Velegol, Multi-ion diffusiophoresis, *J. Colloid Interface Sci.* **424**, 120 (2014).